LANGMUIR

Bulk Phase Behavior vs Interface Adsorption: Specific Multivalent Cation and Anion Effects on BSA Interactions

Madeleine R. Fries, Nina F. Conzelmann, Luzie Günter, Olga Matsarskaia, Maximilian W. A. Skoda, Robert M. J. Jacobs, Fajun Zhang, and Frank Schreiber*
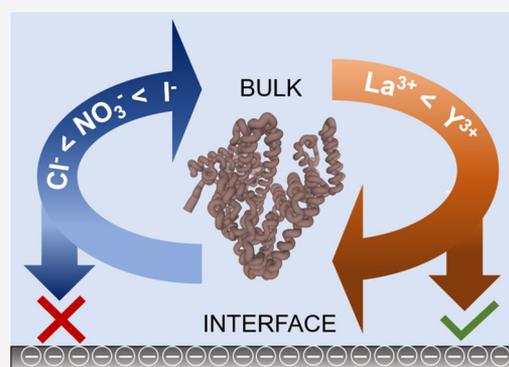
Read Online

ACCESS | Metrics & More | Article Recommendations | Supporting Information

ABSTRACT: Proteins are ubiquitous and play a critical role in many areas from living organisms to protein microchips. In humans, serum albumin has a prominent role in the foreign body response since it is the first protein which will interact with, e.g., an implant or stent. In this study, we focused on the influence of salts (i.e., different cations (Y^{3+}, La^{3+}) and anions (Cl^-, I^-) on bovine serum albumin (BSA) in terms of its bulk behavior as well as the role of charges for protein adsorption at the solid−liquid interface in order to understand and control the underlying molecular mechanisms and interactions. This is part of our group's effort to gain a deeper understanding of protein−protein and protein−surface interactions in the presence of multivalent ions. In the bulk, we established two new phase diagrams and found not only multivalent cation-triggered phase transitions, but also a dependence of the protein behavior on the type of anion. The attractive interactions between proteins were observed to increase from $Cl^- < NO_3^- < I^-$, resulting in iodide preventing re-entrant condensation and promoting liquid−liquid phase separation in bulk. Using ellipsometry and a quartz-crystal microbalance with dissipation (QCM-D), we obtained insight into the growth of the protein adsorption layer. Importantly, we found that phase transitions at the substrate can be triggered by certain interface properties, whether they exist in the bulk solution or not. Through the use of a hydrophilic, negatively charged surface (native silica), the direct binding of anions to the interface was prevented. Interestingly, this led to re-entrant adsorption even in the absence of re-entrant condensation in bulk. However, the overall amount of adsorbed protein was enhanced through stronger attractive protein−protein interactions in the presence of iodide salts. These findings illustrate how carefully chosen surface properties and salts can directly steer the binding of anions and cations, which guide protein behavior, thus paving the way for specific/triggered protein−protein, protein−salt, and protein−surface interactions.

INTRODUCTION

Salts are essential for life as we know it. Humans need to ingest adequate amounts of salts via their diet[1] in order to maintain biological and physiological functions in the body.[2] The absence or excess of salts can lead to diseases such as renal edema, Addison's disease, congestive heart failure,[2] Parkinson's disease,[3] Alzheimer's,[4] or hypertension.[1] For certain bacteria, called halobacteria, a high salt concentration is required for survival,[5] while in plants it can induce cell death due to abiotic stress.[6]

Salts consist of cations and anions, which have different properties and promote ion-specific interactions, thus facilitating different functions in biomolecules, such as proteins, e.g., via ion−protein interactions.[7] To decode their role and more specifically their binding mechanisms to proteins, numerous studies were conducted in the past decades.[8−10] Nevertheless, there are still contradictory opinions and open questions concerning the interplay of ele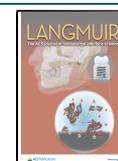ctrostatic, hydrophobic, van der Waals, and entropic interactions between proteins and salts in bulk and at solid interfaces.

The chloride anion (Cl^-) plays a central role in the human body. It is the body's principal anion and the second main contributor to blood plasma tonicity[11] and has a key role in the regulation of body fluids, preservation of electrical neutrality, acid−base balance,[12] muscular activity, and osmotic pressure.[11] In the human body, a chloride imbalance can induce diseases such as dystrophia myotonica, cystic fibrosis, chronic pancreatitis, epilepsy, cataracts, or Barter's disease.[11,13] In addition, it is used to diagnose other diseases and deficiencies.[14] In biopharmaceutical drugs, chloride is, e.g.,
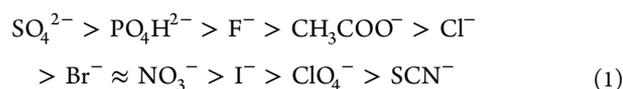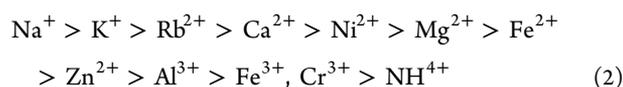
added to liquid antibody solutions for long-term stability[15] or used to study alcohol degradation in the liver.[16]

Another essential anion, which is primarily ingested through fish and dairy products, is iodide (I^-).[17] I^- is, among others such as I_2, I_3, IO^-, HIO, and HI_2O^-, one form of iodine (potentially) present in the human body.[18] In this study, we focus on I^-. It is most prominently known due to its role in thyroid hormone production,[19] but it is also found in the saliva, stomach, intestines, kidneys, ovaries, and bloodstream.[18] An iodide deficiency can lead to goiter and hypothyroidism.[18] Especially during pregnancy, an adequate level of iodide is crucial to prevent mental retardation and cretinism in newborns.[18] In medicine, the antioxidant nature of iodide is used to combat free radicals and peroxides. While it is known for its disinfection/antimicrobial properties,[20] another important aspect is its positive effect in the treatment of cardiovascular diseases,[21] respiratory disorders,[22] inflammatory skin diseases, and especially degenerative eye diseases.[17]

All of these aspects illustrate the importance of studying protein−ion interactions. Some important properties of these interactions are summarized in the so-called Hofmeister series.[23−25] Anions are hereby ordered according to their propensity to salt-in (stabilizing) or salt-out (destabilizing) the protein:

$$SO_4^{2-} > PO_4H^{2-} > F^- > CH_3COO^- > Cl^-$$
$$> Br^- \approx NO_3^- > I^- > ClO_4^- > SCN^- \quad (1)$$

For cations, the corresponding series reads:[25]

$$Na^+ > K^+ > Rb^{2+} > Ca^{2+} > Ni^{2+} > Mg^{2+} > Fe^{2+}$$
$$> Zn^{2+} > Al^{3+} > Fe^{3+}, Cr^{3+} > NH^{4+} \quad (2)$$

Typical physiologically relevant cations are mostly metal ions and have valencies from monovalent (e.g., Na^+) to trivalent (e.g., Al^{3+}) ions.[26] The trivalent lanthanum cation (La^{3+}), which is less known in the physiological context, can be used on the one hand as a model cation due to its similar size to calcium to study, e.g., muscle contraction.[27] On the other hand, it can block unwanted binding of physiological cations with similar size. For example, La^{3+} was found to inhibit the growth of cancerous cells in colon cancer,[28] leukemia,[29] and skin cancer[30] and is thus a component in anticancer drugs already tested in vivo and in vitro.[28] In the same sense, it can act either as a neurotoxin[31] or trigger the release of neurotransmitters.[32] In plants, La^{3+} acts as a chemical fertilizer[33] and relieves the plant of salinity-induced oxidative stress.[34]

Yttrium (Y) belongs to the group of transition metals, but its chemistry is similar to that of lanthanides.[35] Y^{3+} is used in chemotherapy as a treatment for liver cancer[36] and in radioimmunotherapy as part of yttrium-labeled antibodies.[37] In dentistry, elementary yttrium is incorporated into dental implants for better osteoblast adhesion.[38] For a further discussion of selected properties and applications of multivalent ions, see ref 7.

Due to the attractive interaction between opposite charges, cations can bind to negatively charged molecules. Under certain conditions, cations can thereby induce attractive forces, e.g., between macro-anions[39] and bridge particles of equal charge, such as polyelectrolytes,[40] surfactants,[41] or actin filaments.[42] Cations can induce charge inversion in biological membranes,[43] anionic liposomes[44] and globular proteins.[45]

Our group observed a complex phase behavior for globular proteins (human and bovine serum albumins, β-lactoglobulin, ovalbumin) in the presence of multivalent cations such as Cd^{2+}, Zn^{2+}, La^{3+}, Al^{3+}, Y^{3+}, Ho^{3+} and Fe^{3+}.[35,46−50] The phase diagram features phenomena such as liquid−liquid phase separation (LLPS), protein crystallization, and re-entrant condensation (RC) due to cation-induced charge inversion.[35,46−50]

In this study, we focus on the effect of anions (Cl^- vs I^-) and cations (La^{3+} vs Y^{3+}) on the bulk behavior of bovine serum albumin (BSA) as well as on its adsorption behavior on a negatively charged, hydrophilic surface (native silica). Serum albumin is often the first protein to adsorb to a solid interface[51] in contact with blood serum. It is the most abundant blood protein and has a well-studied structure,[52] making it an ideal and important protein to study. In terms of substrate properties, hydrophilic surfaces are highly hemocompatible.[53,54] Negatively charged surfaces are important for initiating blood clotting[55] by inducing protein adsorption and platelet adhesion,[53] besides activating further proteolytic systems in the blood plasma.[56,57] Thus, native silica is a good model surface to study protein adsorption in addition due to its well-defined properties and smooth surface.

In the following, we shed light on the dominant interactions guiding protein cluster formation and protein adsorption and the influence of multivalent salts on these behaviors. We aim to obtain a comprehensive picture of the underlying mechanisms and interactions driving these phase behaviors via ultraviolet− visible (UV−vis) spectroscopy, optical microscopy, Fourier transform infrared spectroscopy (FTIR), and pH measurements. Depending on the ion type, composition, and valency, different protein behaviors are observed due to varying type and strength of interactions. Second, we studied protein adsorption by attenuated total reflectance (ATR)-FTIR, ellipsometry, and quartz-crystal microbalance with dissipation (QCM-D) measurements.

■ EXPERIMENTAL SECTION

Materials and Bulk Phase Behavior. We obtained the materials used in this study from Sigma-Aldrich (now Merck), namely, BSA with a purity of ≥98% (product no. A7906), yttrium chloride (YCl_3) with a purity of 99.99% (product no. 451363), lanthanum chloride ($LaCl_3$) with a purity of 99.99% (product no. 449830), yttrium iodide (YI_3) with a purity of 99.9% (product no. 413011), lanthanum iodide (LaI_3) with a purity of 99.9% (product no. 413674), and deuterium oxide (D_2O) with a purity of 99.9% (product no. 151882). Salt stock solutions with a concentration of 100 mM in degassed Milli-Q water were prepared for the bulk and adsorption measurements. The Milli-Q water has a total organic carbon (TOC) value of 1.7 ppb or μg/L and a resistivity of 18.2 MΩ·cm at 25 °C. BSA has a net negative charge of −10 e at neutral pH.[46] To determine the protein stock solution concentration via the Beer−Lambert law, a UV−vis spectrometer (Cary 50 UV−vis spectrometer, Varian Technologies, USA) was used to perform absorbance measurements. Most proteins containing aromatic amino acids show an absorbance maximum at 280 nm; thus, a range from 200 to 400 nm was scanned for each concentration determination.

For the phase diagram determination, the protein solutions were prepared with degassed Milli-Q water at protein concentrations (c_p) of 1, 2, 5, 20, 50, 80, and 100 mg/mL. The salt concentration (c_s) was varied from 0 to 60 mM. The phase diagrams shown in Figure 1 were determined by eye, UV−vis transmittance measurements, and optical microscopy.[45] The first phase transition from regime I to II at the specific salt concentration c^* is defined by the onset of turbidity (Figures S1 and S2, and Table S1) and LLPS by the formation of a
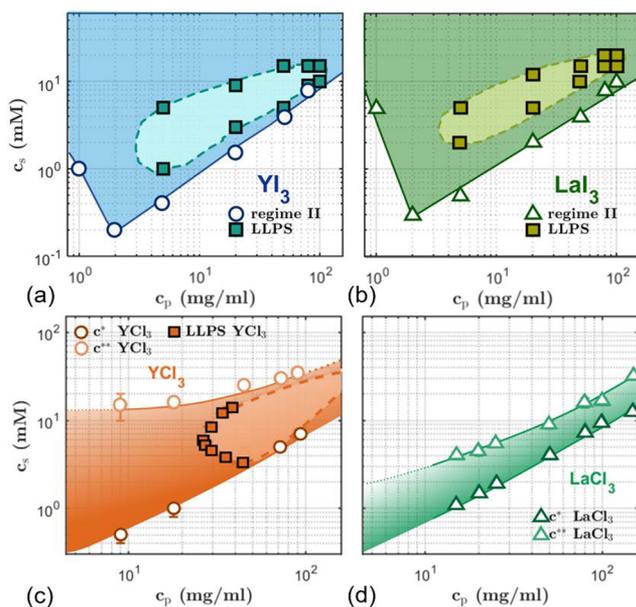
Figure 1. Phase diagrams. BSA phase diagrams at room temperature with (a) YI_3, (b) LaI_3, (c) YCl_3, and (d) $LaCl_3$. The data in (c) and (d) are modified from ref 78. Depending on the salt type, BSA undergoes different phase transitions. All salts, except $LaCl_3$, induce LLPS (square markers). Only the chloride salts lead to re-entrant condensation, whereas BSA in the presence of iodide salts remains in regime II even at high c_s. Note that c^* deviates from a linear slope at very low c_p (1 mg/mL). At low c_p, the intermolecular distances between proteins become very large, thus prohibiting cluster formation until an excessive amount of salt is added. For information on typical pH values and changes in the phase diagram see the pH Changes section and Figure 3.

dilute and dense liquid phase (Figure S1c). More information is provided in the Supporting Information.

pH measurements were performed with the pH/Ion meter S220 of the Seven Compact series from Mettler Toledo (USA). The error can be estimated to be around ± 0.1 due to deviations in pipetting, concentration determination and electrode precision.

FTIR Measurements. FTIR transmittance measurements were performed with a Vertex 70 Fourier transform infrared spectrometer by Bruker (software: OPUS) to get insight into the secondary structure of the protein (clusters) in the different regimes of the bulk solution. We performed a background measurement with the D_2O-filled transmission cell and used the integrated background subtraction tool in OPUS to automatically subtract the background from the sample transmittance measurement. The measurements had to be performed in D_2O due to the overlapping absorbance peaks of H_2O with the amide-I band, which we used as an indicator of the integrity of the secondary structure of proteins. Although Braun et al. have found different phase behaviors for protein/salt systems in D_2O vs H_2O,[58] in the present context D_2O was an appropriate solvent to use since it strengthens protein−protein interactions meaning that since we could not observe any structural changes in D_2O, the weaker interactions in H_2O would not induce changes either. The slight difference between pD and pH values of 0.41 does not influence the overall trend of the results found.[59]

Interface Studies/Adsorption. All adsorption measurements were performed in situ, and the adsorption time was set to 1 h, which was sufficiently close to equilibrium conditions. All samples for ellipsometry and QCM-D were centrifuged and only the supernatant was used (clear solution necessary to perform ellipsometry).

To ensure the reproducibility of our findings and to estimate real standard deviations as statistical error bars, all measurements were repeated at least three times. The systematic errors (e.g., wavelength and angle calibration of the ellipsometer) are substantially smaller

than the statistical error bars. In all figures, the mean value of those measurements with real standard deviation is plotted.

Ellipsometry. The substrates used were p-doped (boron) Si wafers with (100) orientation, which were purchased from Micro-Chemicals GmbH (Germany) (product no. WSM6067525XB1314SNN1). The substrates had a thickness of $675 ± 25 \mu m^2$ and a resistivity of 1−10 Ω·cm. The substrate size was 16 to 8 mm with a native silica layer of roughly 1.7 nm on top, which was measured for each sample individually. The substrates were cleaned with acetone, isopropanol, and water, respectively, for 10 min in each solution in the ultrasonic bath. The contact angle of the substrate with water was around 30°, and the substrate roughness was below 1 nm. We utilized a VASE M-2000 ellipsometer by J.A. Woollam (USA) to perform adsorption measurements with a homemade, solid−liquid cell at 68°, the Brewster angle of native silica in water.[60−62] For data collection and analysis, we used the CompleteEASE software of J. A. Woollam by creating a model including the optical properties of the individual layers. Specifically for BSA, a Cauchy layer with $A = 1.43$, $B = 0.01$, and $C = 0$ was chosen (in the literature, the value of A varies between 1.42 and 1.45 for BSA).[63−66]

QCM-D Measurements. QCM-D measurements were conducted with the Q-Sense Analyzer of Biolin Scientific (Sweden).[67−69] The measurements were performed with the QSoft software and analyzed with Dfind and QTools of Biolin Scientific. The quartz sensors used were native silica-coated (product no. QS-QSX303). The flow cell allowed in situ cleaning with 2% Hellmanex, ethanol, and water. The setup had the option of inverting the cell with the substrate on top of the solution, which was utilized, thus avoiding sedimentation effects. Since the dissipation (D) was greater than 0, a viscoelastic (Voigt) model was used for the data analysis of BSA. If the viscoelastic properties of the adsorbed material are too pronounced, the oscillating sensor gets damped too strongly ($D \neq 0$) and the direct correlation between frequency drop and mass uptake described by the Sauerbrey model is not valid anymore.[70] For more information on the Voigt model, see refs 68, 71, and 72. In combination with the ellipsometer, we were able to determine the associated water (d_{assoc}) within our adsorption layer.[73,74] Since ellipsometry does not account for the water content in the adsorbed protein layer thickness determined (d) and the QCM-D cannot differentiate between water and proteins adsorbed to the interface, the extracted adsorbed layer thickness d_{QCM-D} contains both. More details on data analysis and fitting parameters can be found in ref 75.

ATR-FTIR Measurements. ATR-FTIR measurements allow for structure determination of adsorbed proteins to a solid interface and were conducted with the Thermo Nicolet iS50 with Specac Gateway ATR insert.[76,77] The measurement software was Omnic, and the following settings were chosen for the absorbance measurements on the Si block: gain, 1; aperture, 10; scan no., 294; resolution, 4 cm^{-1}. The evanescent wave penetrates through the substrate a few micrometers into the bulk solution. Thus, the measured signal contains not only the adsorbed proteins but also the signal of the surrounding bulk proteins. To check for the influence of the bulk proteins on the absorbance data, we flushed the cell and checked if the signal of the reversibly adsorbed proteins in water changed compared to the adsorption layer in bulk, which was not the case (Figure S6). The measurements were conducted in H_2O, but checks were made in D_2O (data not shown), to ensure the background subtraction was sufficient even though the H_2O and amide-I signals are overlapping. The data were corrected for the background, but not for the baseline, which explains the small offset at 0 absorbance of the individual curves (Figure 5). The slight differences in the amide-II band and amide-I peak position compared to the FTIR measurements shown in Figure 2 are due to the use of H_2O as the solvent instead of D_2O.

■ RESULTS AND DISCUSSION

We studied the effect of different anions and multivalent cations on the protein bulk phase behavior and the adsorption
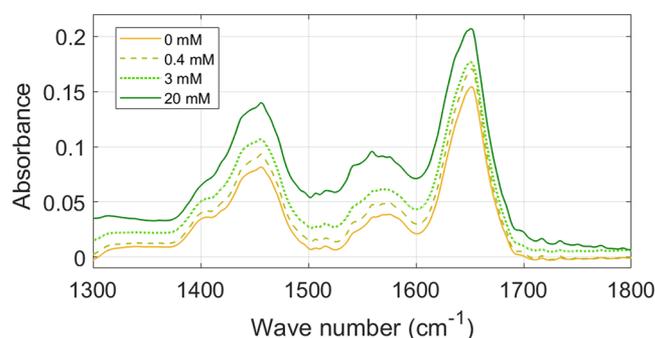
Figure 2. Secondary structure of BSA. FTIR transmittance measurements of the BSA/LaI$_3$ system at c_p = 20 mg/mL and 20 °C in D$_2$O. The measurements cover all regimes showing no significant changes in the amide-I band (1600−1700 cm^{-1}) at c_s of 0, 0.4, 3, and 20 mM salt. Note that the slight differences in peak intensity and position in amide-II are due to incomplete water subtraction from transmittance measurements. The complete FTIR spectra can be found in Figure S4.

behavior at a solid−liquid interface. In the following, we will present the phase behavior of BSA in the presence of YCl$_3$, LaCl$_3$, YI$_3$, and LaI$_3$, which differs depending on the anion and cation type in the bulk solution. The phase diagrams in the presence of chloride salts were already established in previous publications by Matsarskaia et al.[35] and Braun et al.,[78] and they are used as a reference for the protein adsorption measurements and the newly established phase diagrams of LaI$_3$ and YI$_3$.

Phase Diagrams. First, we focus on the anion iodide and its influence on the protein bulk phase behavior. We establish the phase behavior of BSA with YI$_3$ and LaI$_3$ at room temperature (Figure 1a and b). Both phase diagrams show a first phase transition from regime I (transparent) into regime II (turbid) at a given salt concentration c* and a metastable liquid−liquid phase separation (LLPS) region (square symbols in Figure 1), which starts to occur at $c_p \sim$ 5 mg/mL, i.e., within regime II. pH changes are occurring, but they are not the dominant force driving the phase behavior. More information is provided in the pH Changes section. This phase behavior of globular proteins mixed with multivalent ions has been first established by Zhang et al.[45] and can be rationalized as follows. The initially net negative charge of the proteins is neutralized by the addition of salt in regime I.[45,47] At a specific salt concentration c*, the dominant force changes from repulsive to attractive due to the binding of trivalent cations to negatively charged patches of the protein. The cations can even bridge proteins, thus promoting protein aggregation (regime II).[79] The binding mechanism between cations and proteins can be rationalized by electrostatic interactions.

In colloid-like systems, including protein solutions, LLPS can occur depending on the interaction strength between particles. One parameter to determine the interaction strength and type is the reduced second virial coefficient B_2/B_2^{HS}, where B_2^{HS} is the second virial coefficient of hard spheres.[80] A threshold value of B_2/B_2^{HS} determined for LLPS formation in colloid theory is −1.5.[58,80] LLPS forms at lower c_s and extends to higher c_s for BSA with YI$_3$ than with LaI$_3$. In addition, c* is lower in the presence of YI$_3$ than LaI$_3$.

These differences in BSA phase behavior induced by Y^{3+} and La^{3+} can be rationalized by weaker protein−protein interactions and cation−protein binding properties of La^{3+}. The cation radius[81,82] and hydration effects[83,84] contribute to

the effective protein−protein interactions. While other mechanisms may also play a role, it is reasonable to assume that the bigger the cation (lower charge density), the weaker are the attractive interactions it can induce. A detailed study on the role of cations on the BSA phase behavior was performed by Matsarskaia et al.[35] Our findings are consistent with the previous work on chloride salts illustrated in Figure 1c and d.
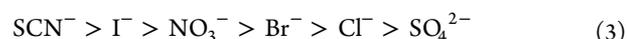
Interestingly, no re-entrant condensation occurs with either iodide salt. This implies that no transition into regime III is observed and thus at high c_s the protein-salt solution remains in regime II. Additionally, in the case of the iodide salts, LLPS begins at lower c_p compared to BSA in the presence of chloride salts (Figure 1c and d). This indicates much stronger BSA−BSA attractive forces in the presence of iodide salts, for which protein−protein interactions are attractive even at very high c_s. This behavior is in good agreement with the behavior found for BSA with nitrate salts. Note that the respective phase diagrams of BSA with nitrate salts are shown in Figure S3 as a reference for the reader. Braun et al.[78] already observed attractive interactions of BSA at very high c_s, in their case with nitrate salts (LaNO$_3^-$ and YNO$_3^-$), indicated by the phase diagram and measured B_2/B_2^{HS} values. A systematic change in phase behavior of BSA with Cl$^-$, NO$_3^-$, and I$^-$ can be observed: c* shifts to higher c_s, LLPS occurs at lower c_p, and RC vanishes. Thus, ranking the anions from inducing strong attractive interactions from weakest to strongest: Cl$^-$ < NO$_3^-$ < I$^-$. Multiple factors contribute to this behavior, which are explained in the following sections and supported by relevant anion properties in Table 1.

Table 1. Properties of Anions^a

parameter	chloride (Cl$^-$)	nitrate (NO$_3^-$)	iodide (I$^-$)
effective anion radius,[85,86] r_{ion} (Å)	1.8	2.0	2.2
heat capacity,[86] $C_{p,str}$ (J/(K·mol))	−237	−234	−288
ionic aqueous surface tension,[85] dγ/dc_i (mN/(m·M))	0.90	0.15	−0.05
Jones−Dole ionic B coefficient,[86−89] B (dm^3/mol)	−0.007	−0.046	−0.068
number of bound ions to BSA at pH 5,[90] n_{ion} (#)^b	8	19	48
structural entropy,[86,88] S_{str} (J/(K·mol))	58	66	117
water structure parameter,[85,88,91] ΔG_{HB}	−0.61	−0.68	−1.09

^{a}Important parameters, which influence the ion-water and ion-protein interactions relevant for this study. ^{b}The concentration of added anion was 0.1 mol/kg and the protein concentration ≈ 0.3 mM, which is equivalent to our used protein concentration of 20 mg/mL.

Hydration and Protein Stability. According to the Hofmeister series, iodide is more prone to cause destabilization of the protein (denaturation) than chloride,[92] which could prevent re-entrant condensation (c**). Yet, at low and moderate ionic strengths (<0.1 M), weakly hydrated anions such as iodide neutralize the electrostatic repulsive forces and thermostabilize BSA more efficiently than strongly hydrated anions, leading to the reverse Hofmeister series:[93−95]

$$\text{SCN}^- > \text{I}^- > \text{NO}_3^- > \text{Br}^- > \text{Cl}^- > \text{SO}_4^{2-} \qquad (3)$$

This order is based on the hydration of an ion, which is linked to its ion radius, heat capacity $C_{p,str}$, ionic B coefficient B, and structural entropy S_{str} listed in Table 1. These properties also determine whether the ion is making or breaking the water structure around itself according to Marcus[85,86,88] and can be

expressed with the water structure parameter ΔG_{HB}.[91] Thus, in this c_s range (<0.1 M), iodide stabilizes the BSA structure better than nitrate and nitrate does so better than chloride. In fact, Cl$^-$ is known to have little effect on the water structure or protein stability[96,97] and thus has a passive role in this context.

In order to assess the influence of iodide on the secondary structure of BSA, FTIR measurements were performed (see Figure 2). The secondary structure of BSA is stable over a LaI$_3$ concentration range from 0 to 20 mM with a prominent peak around 1650 nm^{-1} in D$_2$O (amide-I). This peak is associated with α-helices, which make up roughly 66% of BSA in its native shape[98] and indicates an intact globular structure. Performing multiple measurements at different c_s values of 0, 0.4, 3, and 20 mM did not show any significant structural changes in the amide-I band due to salt type or concentration. Thus, we can exclude that denaturation or strong structural changes in the protein structure are the cause for the suppression of re-entrant condensation, i.e., the absence of regime III.

pH Changes. The addition of salt and subsequent salt-induced water hydrolysis and ionization of hydrophilic protein residues[99] can change pH and thus, in principle, protein behavior. Importantly, though, previous studies have shown that the trivalent cations (Y^{3+} and La^{3+}) used here do not induce significant pH changes.[99] To determine the effect of anions on the pH, the pH of BSA-LaI$_3$ samples was measured after preparing the protein/salt mixtures (Figure 3). The pH
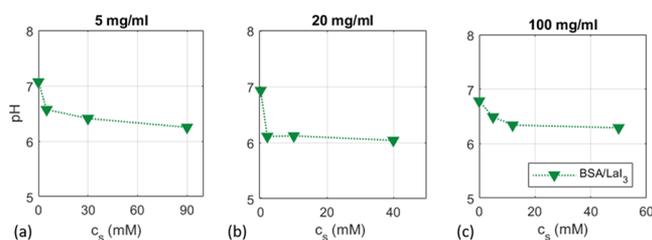

Figure 3. Bulk pH measurements of the BSA/LaI$_3$ system. Measurements were performed at c_p = (a) 5, (b) 20, and (c) 100 mg/mL with varying c_s. The precision of this method can be estimated around pH $\pm$ 0.1. These pH changes are similar to those of pH-neutral salts (i.e., YCl$_3$ and LaCl$_3$).[99]

decreases slightly with increasing salt concentration, yet the drop in pH does not correlate with the phase transitions seen in the bulk. The pH does not change significantly with time or c_p either. This pH trend of LaI$_3$ is similar to that found for YCl$_3$ in our previous publication[75] as well as similar to the pH variations of pH-neutral salts (i.e., YCl$_3$ and LaCl$_3$).[99] We thus conclude that, while pH effects may contribute to the protein phase behavior in some form, they do not qualitatively change the bulk behavior and are not primarily responsible for the absence of regime III observed with iodide salts as opposed to the chloride salts.

Amount of Anions Bound to BSA. The literature consistently reports that more iodide anions are bound to BSA per molecule than nitrate ions and even less chloride anions (see Table 1).[90,100] If the number of anions bound depends on the anion type, it can explain why a certain anion type has a stronger influence on the protein phase diagram than another, which results, e.g., in the disappearance of re-entrant condensation. The number of anions bound increases as Cl$^-$ < NO$_3^-$ < I$^-$, which reflects the order of ion-induced attractive interactions in the phase diagram. Thus, it is reasonable to assume that iodide has a stronger influence on

protein−protein interactions, which again emphasizes the general weak effect of Cl$^-$ on the protein stability or water structure.[96,97]

To obtain a comprehensive understanding on the different binding affinities of anions to BSA, different mechanisms and properties leading to the binding affinity are described and discussed in the following sections.

Strength of Protein−Ion Interaction. Weakly hydrated anions bind directly to proteins, causing the protein to maximize its solvent accessible surface area and the bulk solution to become a better solvent.[101] In turn, strongly hydrated anions interact indirectly through bound water molecules with the protein, thus reducing the proteins surface area by making it more compact. The bulk solution becomes a worse solvent.[101] Anions with a lower charge density bind more tightly to the protein. This implies that iodide binds more tightly to BSA than nitrate and nitrate stronger than chloride (see Table 1 for anion radius and surface charge).[101] In other (positively charged) proteins, it was found that iodide can bridge proteins, thus promoting anion-induced cluster formation.[102,103] One indicator for iodide-mediated protein−protein bridging, as well as cation bridging of BSA molecules in solution, is that, at high c_s for both LaI$_3$ and YI$_3$, the protein cluster sizes increase until they start to sediment at c_s > c_s(LLPS) and the volume of "dense" (sedimented) protein phase further increases with increasing c_s (Figure S1a and b). This is also inversely reflected in the c_p values of the "dilute" (upper) phase, which decreases with increasing c_p (Figure S5). The *combination* of increased c_p and volume of the sedimented phase indicates consistently attractive interactions between proteins even at high c_s, preventing re-entrant condensation. This is consistent with results by Braun et al.[78] for BSA/La(NO$_3$)$_3$, which found stable B_2/B_2^{HS} values at −2.25 for high c_s and c_p, at which re-entrant condensation vanished. In systems in which re-entrant condensation is always present (i.e., LaCl$_3$ and YCl$_3$), the B_2/B_2^{HS} values start to increase at high c_s, illustrating the decreasing attractive force due to cation-induced overcharging effects of the proteins. The decreased c_p of the dilute phase of YI$_3$ compared to LaI$_3$ further supports the finding of stronger BSA−BSA interactions in the presence of Y^{3+} and is consistent with the trend found for LaCl$_3$ compared to YCl$_3$ by Braun et al.[78]

Binding Sites. The literature distinguishes between specific and nonspecific, high and low affinity, and polar and nonpolar ion-binding sites on proteins. It appears to be established that chloride binds to cationic/basic binding sites of BSA[93,104] and HSA,[105−107] which are specific and high-affinity binding sites, whereas there are numerous and contradictory opinions on the binding of iodide. Some studies do not discriminate between anion type and thus assume the same binding mechanism for iodide to positively charged protein groups of BSA,[93,104] while others find a different (nonspecific) binding mechanism for iodide to nonpolar groups of HSA,[107] lysozyme,[102,108,109] human carbonic anhydrase II,[110] and peptide.[111] The same applies to the binding of other anions such as anionic dyes,[112] anionic amphiphiles,[113] or anionic ligands[114] to BSA, all of which bind preferentially to hydrophobic groups. In some cases, an interplay of electrostatic and hydrophobic inter-actions is needed, in which the proximity of positive and nonpolar groups has a favorable effect on anion bind-ing.[107,113,115] BSA has numerous binding sites with different binding affinities due to specific and nonspecific binding mechanisms. In any case, the binding mechanism of iodide is

much more complex than the binding of chloride.[105] Chloride binds only to positively charged sites, whereas, depending on the bulk properties (i.e., charge and polarity of protein), iodide will bind specifically to positively charge sites and/or nonspecific to hydrophobic sites with different affinities.[104,110,116] In comparison, multivalent cations bind to acidic areas (surface-exposed carboxylic groups)[79,117,118] on the protein via an endothermic, electrostatically and entropy-driven process.[119]

Competing Interactions. In addition to the properties of the anion, the trivalent cations have to be considered as well. Anion−cation chloro-complex formation can be excluded since those start to form at 0.2 M for yttrium salts and 0.4 M for lanthanum salts, respectively.[120−123] Nitrato-complexes start to form at 0.12 M for lanthanum salts and 0.18 M for yttrium salts,[122,123] which are c_s values outside of the phase diagram shown in Figure 1. Iodo-complexes start to form at lower c_s than chloro-complexes, yet this should not influence our measurements.[124] Thus, anion−cation complexes do almost certainly not contribute to the effects studied. However, anions could assist and amplify the effect of cations on protein−protein interactions.[111,125] Depending on the cation type and charge of the protein in system, the anion can support the destabilizing or stabilizing role of the cation on the protein structure.[111,125]

Overall, electrostatic (and hydrophobic) ion−protein and protein−protein interactions and the special role of multivalent ions are key for the understanding of the observed (bulk) behavior. The increasing role and effect of anions from Cl^- < NO_3^- < I^- on the phase diagram can be explained with the combination of an increasing number of ions bound to BSA, stronger binding, increasing protein-stabilizing role of ions, potentially anion bridge formation and increasing role of nonspecific protein−protein interactions, as well as cation bridges. These properties appear to be responsible for preventing the system from undergoing re-entrant condensation triggered by trivalent cations, which means that it remains in regime II with dominant attractive forces between protein molecules, for the iodide salts and partially for nitrate salts.

Protein Adsorption. In this section, we discuss how the presence of different salts ($LaCl_3$, YCl_3, LaI_3, YI_3) in BSA solutions (c_p = 20 mg/mL) influences the adsorption behavior of BSA to a net negatively charged, hydrophilic substrate and to which extent this is related to the bulk protein phase behavior.

Salt-Dependent Protein Adsorption (Ellipsometry). The thickness of the adsorbed amount of BSA on native silica, d, is plotted as a function of ratio of salt/protein concentration (c_s/c_p) in Figure 4. The effective measured d with ellipsometry assumes a volume fraction of 1, which is laterally averaged over the measured surface.

Different aspects need to be considered when comparing the different adsorption trends. These include the position of the adsorption maximum, the amount of protein adsorbed, and the overall shape of the curve. Without salt, adsorption of $d \approx 1$ nm can be observed. This can be attributed to positively charged side chains of the protein interacting with the negatively charged substrate, as well as contributing hydrophobic and hydrogen bond interactions,[127] leading to sparse adsorption at the interface.

The initial increase of adsorption can be ordered according to LaI_3 < $LaCl_3$ < YI_3 < YCl_3 shown in the inset of Figure 4, meaning that the smallest amount of YCl_3 is needed to achieve
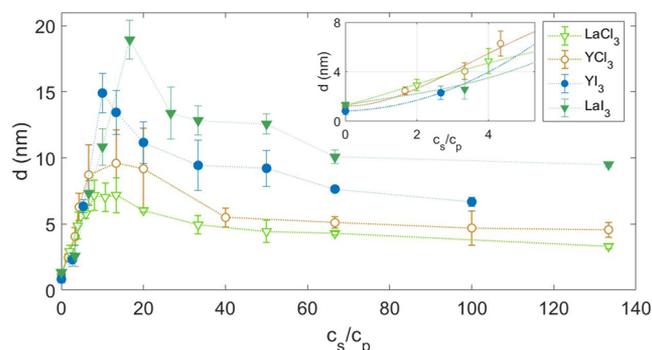

Figure 4. Ion effect on protein adsorption. Ellipsometric measurements of the adsorbed protein layer thickness d as a function of c_s/c_p at 20 mg/mL BSA and room temperature for $LaCl_3$ (light green), YCl_3 (orange), YI_3 (blue), and LaI_3 (dark green). The data for YCl_3 is taken from ref 126. The absolute value of d increases as $LaCl_3$ < YCl_3 < YI_3 < LaI_3. For better visibility, the inset shows a magnification of the initial adsorption increase from 0 to 5 c_s/c_p together with a guide to the eye.

the thickest adsorption layer at low c_s. This behavior reflects the bulk phase transition c^* from regime I to regime II at 2 > 1.5 ≈ 1.5 > 1.3 mM salt, respectively, which occurs at lower c_s for the yttrium salts than for the lanthanum salts due to the stronger attractive intermolecular forces induced by Y^{3+} (see Figure 1). For iodide salts, more salt has to be added to the protein solution to observe the transition from regime I to II at c^* than for chloride salts. This is due to the fact that iodide has a dominant role in the protein behavior hindering "simple" charge screening through multivalent cations in bulk and at the interface.

The shape of the adsorption curve maximum is similar to that of the bulk interactions. In bulk, regime II of the BSA−$LaCl_3$ system is very narrow compared to that of YCl_3 (Figure 1c), which is reflected in the width of the maximum. For the iodide salts, the LLPS regime starts at a lower c_s (3 mM) for YI_3 than for LaI_3 (5 mM) (Figure 1a and b). This bulk instability induces stronger adsorption, explaining the position of the curve maximum (Figure 4).

Another interesting observable is the maximum adsorbed amount, which follows the order $LaCl_3$ < YCl_3 < YI_3 < LaI_3. The weaker adsorption for $LaCl_3$ in comparison with YCl_3 is due to weaker attractive protein−protein[35] and subsequently protein−substrate interactions. The general adsorption trend of $LaCl_3$ and YCl_3 can be explained using the ion-activated attractive adsorption model.[126] It assumes negatively charged patches on the protein and the substrate to which cations can bind and also form ion bridges between protein molecules and between protein and substrate. In this context, the model neglects the anions (here: chloride), since they have no strong impact on the overall bulk[99] or adsorption behavior. Adsorption is guided by the number of multivalent cations bound to the proteins and the substrate and an attractive wall potential experienced by the proteins.[126] This obviously applies to both $LaCl_3$ and YCl_3.

The iodide salts show higher maximum adsorption in comparison to the chloride salts. It is important to bear in mind that the iodide salts induce a strong LLPS in regime II in the bulk solution (Figure 1). In a previous publication, we studied the correlation of metastable LLPS formation (i.e., bulk instability) in bulk with enhanced protein adsorption[75] and found a wetting transition induced by LLPS at the solid
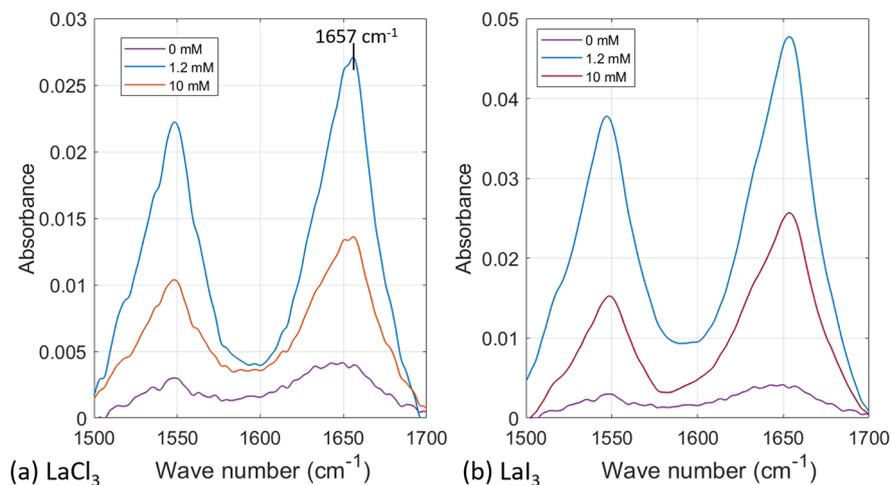
Figure 5. Structure of adsorption layer. ATR-FTIR measurements of 5 mg/mL BSA in H_2O on native silica substrates for (a) $LaCl_3$ and (b) LaI_3 at no salt, 1.2, and 10 mM, respectively.
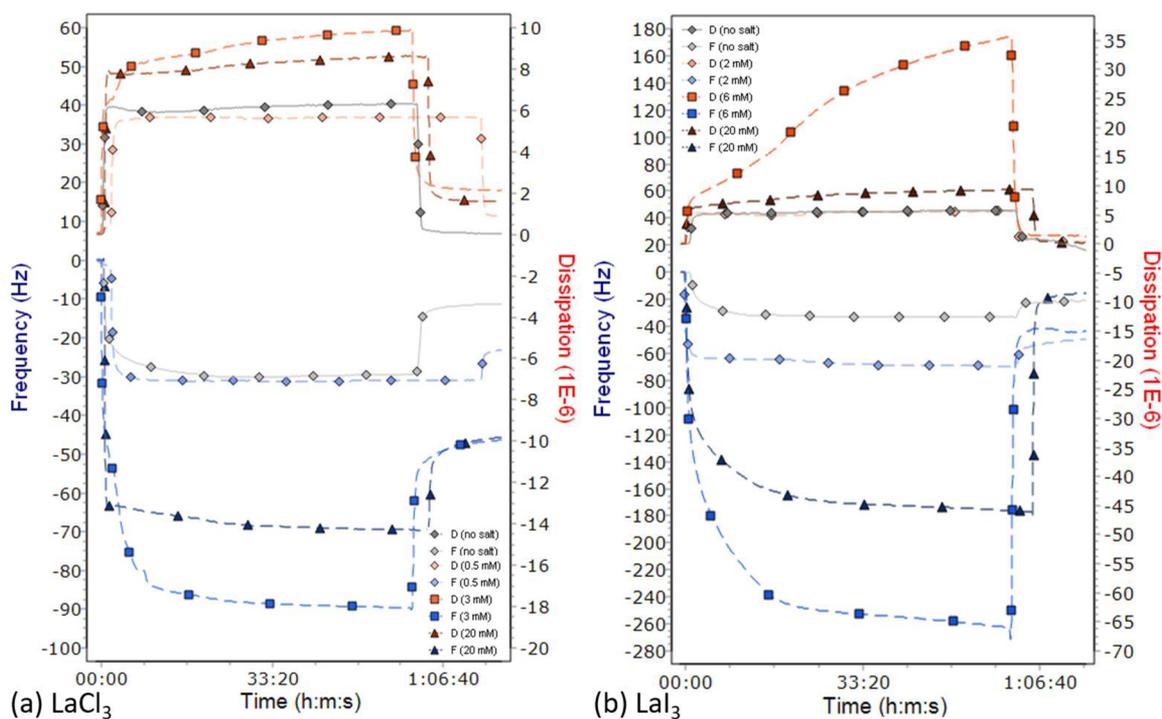

Figure 6. Real-time adsorption data. QCM-D frequency and dissipation changes during protein adsorption of 20 mg/mL BSA at room temperature with (a) $LaCl_3$ and (b) LaI_3 at different c_s reflecting the adsorption behavior in the different regimes. Note that only the ninth overtone of each measurement is shown for better clarity. Initially, the cell is filled with water, and then the protein/salt solution is pumped in and measured for 1 h, after which the cell is flushed with water to check for irreversible protein adsorption.

interface for BSA with YCl_3. These results are in good agreement with our findings and further support the wetting layer transition at bulk instability also for iodide salts. Here, LaI_3 leads to more pronounced adsorption compared to YI_3, which appears counterintuitive at first. Even though yttrium induces stronger interprotein attraction, it appears that this trend is reversed if the counterion is iodide. This shows that the ion-activated adsorption model cannot be applied to the iodide salts since the iodide anions compared to chloride ions have a strong impact on the phase behavior, as well as on adsorption, and the model does not account for the anions in solution. Note that in regime II only the dilute phase can be used for ellipsometry measurements. The dilute phase shows a

c_s-dependent decrease in c_p (see Figure S5). This effect may contribute in some form to the smaller amount of adsorbed protein in the presence of YI_3 compared to LaI_3, but it does not alter the dominant interaction and interaction strength of the bulk solution. It seems that a "stronger" cation such as Y^{3+} induces interactions which interfere with and diminish the effect of iodide. However, with a "weaker" cation such as La^{3+}, iodide has a more prominent effect on the amount of protein adsorbed, indicating a pronounced formation of anion bridges and nonspecific protein–protein binding.

At high c_s, we observe re-entrant adsorption for all salts. For the chloride salts, this was expected since these salts undergo re-entrant condensation at c^{**} from regime II to regime III in

the bulk, which is defined by charge inversion of the proteins due to trivalent cation binding[48] and thus a decrease in attractive forces leading to smaller clusters and to a decrease in adsorption. These results are consistent with previous findings in polyelectrolytes[128] and proteins[75] and can be explained with the ion-activated adsorption model.[126] For the iodide salts, re-entrant *condensation* in the bulk was not observed. Re-entrant *adsorption* on a solid interface, however, was observed. For a hypothesis rationalizing this behavior, it helps to consider the possible protein−protein vs protein−surface interactions. Due to the surface being negatively charged and hydrophilic, anions are not likely to bind to the substrate with high surface excess since iodide prefers to adsorb to nonpolar and/or positively charged surfaces.[93,102,104,107,109] This means that, in the vicinity of the substrate with restricted properties, charge inversion mediated by trivalent cations can occur. In the bulk, in contrast, this is not the case due to the complex protein surface of BSA containing nonpolar, polar, negatively and positively charged areas. Consequently, the variety of possible protein−protein and protein−salt interactions hinder re-entrant condensation.

Global Protein Structure on Substrate (ATR-FTIR). To exclude denaturation at the interface as the primary source for re-entrant adsorption at high c_s, we performed ATR-FTIR measurements on BSA in the presence of LaCl$_3$ and LaI$_3$ on a Si block (Figure 5), which showed essentially intact secondary protein structures. Both salts showed maximum absorbance at 1657 cm^{-1}, which correlates with its dominant α-helix structure.[129] The absorbance signal is much more intense for LaI$_3$, which can be explained by an increased adsorption compared to LaCl$_3$ and is consistent with the ellipsometry findings. The amide-I band does not significantly change its shape with increasing concentration of the same salt, but it differs slightly between the two salts.

Protein Layer Structure and Kinetics (QCM-D). Complementary measurements were conducted with QCM-D, which on the one hand confirmed the results of our ellipsometry data and on the other hand provided additional insights into the structure and properties of the adsorption layer.[130,131] For data analysis, we used the Voigt viscoelastic model[68,132−134] to calculate the thickness of the adsorbed layer from the measured frequency and dissipation changes (for examples of raw data, see Figure 6). Already from the raw data, the difference between LaCl$_3$ and LaI$_3$ is obvious. For all samples in the presence of the respective salt, the frequency drop is lower in the presence of LaI$_3$. This means that more proteins are adsorbed to the substrate, leading to a stronger damping of the oscillating substrate compared to the same c_s of LaCl$_3$. In addition, the dissipation is higher in the LLPS regime, indicating a more diffuse layer formation. Similar to the ellipsometry data (Figure 4), we observe re-entrant adsorption for both data sets. The calculated adsorbed protein layer thickness d_{QCM-D} is plotted in Figure 7a. The overall adsorbed d_{QCM-D} of BSA/LaI$_3$ is enhanced compared to LaCl$_3$, which is in good agreement with the results shown in Figure 4. By rinsing the QCM-D cell with water, the amount of irreversibly adsorbed proteins was determined (Figure 7, black symbols). These make up only a small portion of the full adsorption layer of roughly 10 nm and can be assumed to be the first monolayer of proteins directly in contact with the substrate.

A big advantage of QCM-D in combination with ellipsometry is that we are able to determine the associated water d_{assoc} within our adsorption model (Figure 7b).[73,74] The
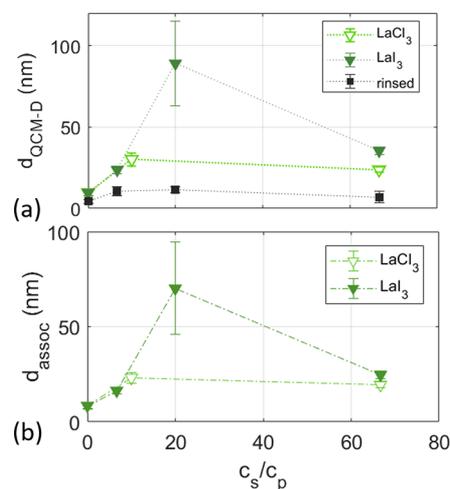
Figure 7. BSA adsorption with associated water content. (a) d_{QCM-D} as a function of salt concentration at 20 mg/mL BSA and room temperature with LaCl$_3$ (light green), LaI$_3$ (dark green), and LaI$_3$ rinsed with water (black). (b) Associated water d_{assoc} reflects the water content within the adsorption layer, which is calculated by subtracting the ellipsometer data from the QCM-D data. The enhanced adsorption of LaI$_3$ is due to a bulk instability (LLPS) and the subsequent formation of a wetting layer. Note that the offset between the two maxima is due to the different positions of regime II in the bulk.

associated water consists of a hydration layer around the proteins, hydro-dynamically bound water to the substrate and water trapped within the adsorption layer.[135] With the information on the water content in the adsorption layer, the layer morphology can be better understood. In a previous publication,[75] we established experimentally and theoretically the correlation between the formation of a wetting layer at the bulk instability induced by LLPS, which exceeded simple "stronger adsorption". Here, only LaI$_3$ leads to LLPS in regime II and thus induces enhanced adsorption. The calculated associated water content is massively enhanced at $c_s/c_p = 20$, which reflects the onset of a enhanced adsorption (wetting transition) compared to a "normal" adsorption layer in regime I and III and therefore is consistent with our previous findings of BSA/YCl$_3$.[75] This is also reflected in the changed viscoelastic properties and higher water content in the adsorbed protein layer in regime II. Besides this concentration in regime II, the water content in the adsorbed layer is comparable between these two salts assuming the same layer morphologies and only enhanced adsorption in the presence of iodide salts.

■ CONCLUSIONS

In this study, we focused on the effect of anions and cations on the protein bulk behavior and adsorption behavior. Interestingly, we reveal that the co-ion (anion) changes the balance and weakens the effect of trivalent cations in the bulk, making re-entrant condensation disappear and liquid−liquid phase separation appear. Chloride does not appear to significantly affect the phase diagram of BSA, whereas iodide promotes stronger attractive protein−protein interactions. This illustrates a dominant role of anions on the phase behavior of globular proteins in the presence of multivalent cations.

By choosing specific substrate properties (here: imitating the bulk properties), the influence of ions on protein adsorption can be controlled. In the BSA−YCl$_3$ system studied in ref 126,

the bulk and adsorption behavior were highly similar due to the negative charge of the proteins, as well as the substrate, and the passive role of chloride. By extending this study to salts with different cations and anions, we have shown that the adsorption behavior is not solely guided by the dominant electrostatic bulk interactions but can also be triggered by surface parameters. This explains the observations presented here: re-entrant adsorption in the absence of re-entrant condensation in bulk. The higher adsorbed amount supports the dominant role of iodide and the hypothesis of anion bridging and nonspecific binding in bulk.

Through the use of suitable anions and cations, the dominant interactions in bulk can be tuned, while in the adsorption process substrate properties can effectively reduce or even uncouple those interactions. The regulation of interactions on a molecular level opens up new avenues for drug design and biomaterials. In addition to its medical relevance, the use of iodide is potentially very useful for studies of our system using X-rays due to its high scattering power and contrast with light elements (i.e., water and proteins).

■ ASSOCIATED CONTENT

Ⓢ Supporting Information

The Supporting Information is available free of charge at https://pubs.acs.org/doi/10.1021/acs.langmuir.0c02618.

Phase transition determined by UV−vis transmittance measurements; dilution series and bulk microscopy images; UV−vis transmittance measurements; BSA phase diagram in the presence of nitrate salts; complete FTIR absorbance spectrum; protein concentration of dilute phase; ATR-FTIR absorbance measurements after rinsing (PDF)

■ AUTHOR INFORMATION

Corresponding Author

Frank Schreiber − *Institute for Applied Physics, University of Tübingen, 72076 Tübingen, Germany; Center for Light-Matter Interaction, Sensors & Analytics LISA⁺, University of Tübingen, 72076 Tübingen, Germany;* ◉ orcid.org/0000-0003-3659-6718; Email: frank.schreiber@uni-tuebingen.de

Authors

Madeleine R. Fries − *Institute for Applied Physics, University of Tübingen, 72076 Tübingen, Germany;* ◉ orcid.org/0000-0002-9643-9215

Nina F. Conzelmann − *Institute for Applied Physics, University of Tübingen, 72076 Tübingen, Germany*

Luzie Günter − *Institute for Applied Physics, University of Tübingen, 72076 Tübingen, Germany*

Olga Matsarskaia − *Institut Max von Laue - Paul Langevin (ILL), F-38042 Grenoble, France;* ◉ orcid.org/0000-0002-7293-7287

Maximilian W. A. Skoda − *ISIS Facility, STFC, Rutherford Appleton Laboratory, Didcot, Oxon OX11 0QX, United Kingdom*

Robert M. J. Jacobs − *Department for Chemistry, University of Oxford, Oxford OX1 3TA, United Kingdom*

Fajun Zhang − *Institute for Applied Physics, University of Tübingen, 72076 Tübingen, Germany;* ◉ orcid.org/0000-0001-7639-8594

Complete contact information is available at:

https://pubs.acs.org/10.1021/acs.langmuir.0c02618

■ ABBREVIATIONS

Y^{3+}, yttrium cation; La^{3+}, lanthanum cation; Cl^-, chloride anion; I^-, iodide anion; NO_3^-, nitrate anion; BSA, bovine serum albumin; QCM-D, quartz-crystal microbalance with dissipation monitoring; SiO_2, silicon dioxide; LLPS, liquid−liquid phase separation; RC, re-entrant condensation; FTIR, Fourier transform infrared spectroscopy; ATR, attenuated total reflectance; HSA, human serum albumin; B_2/B_2^{HS}, reduced second virial coefficient; c_s, salt concentration; c^*, first phase transition; c^{**}, salt concentration of re-entrant condensation; c_p, protein concentration; r_{ion}, effective ion radius; $C_{p,str}$, heat capacity; $d\gamma/dc_i$, ionic aqueous surface tension; B, Jones−Dole ionic B coefficient; S_{Str}, structural entropy; ΔG_{HB}, water structure parameter; d, adsorbed protein layer thickness; d_{QCM-D}, adsorbed protein layer thickness via QCM-D; d_{assoc}, associated water in the adsorbed layer

■ REFERENCES

(1) Boegehold, M. A.; Kotchen, T. A. Importance of dietary chloride for salt sensitivity of blood pressure. *Hypertension* **1991**, *17*, I158.

(2) Grollman, A. The role of salt in health and disease. *Am. J. Cardiol.* **1961**, *8*, 593−601.

(3) Gaetke, L. M.; Chow, C. K. Copper toxicity, oxidative stress, and antioxidant nutrients. *Toxicology* **2003**, *189*, 147−163.

(4) Rondeau, V.; Commenges, D.; Jacqmin-Gadda, H.; Dartigues, J.-F. Relation between aluminum concentrations in drinking water and Alzheimer's disease: an 8-year follow-up study. *Am. J. Epidemiol.* **2000**, *152*, 59−66.

(5) Lanyi, J. K. Salt-dependent properties of proteins from extremely halophilic bacteria. *Bacteriol. Rev.* **1974**, *38*, 272.

(6) Yan, S.; Tang, Z.; Su, W.; Sun, W. Proteomic analysis of salt stress-responsive proteins in rice root. *Proteomics* **2005**, *5*, 235−244.

(7) Matsarskaia, O.; Roosen-Runge, F.; Schreiber, F. Multivalent ions and biomolecules: Attempting a comprehensive perspective. *ChemPhysChem* **2020**, *21*, 1739.

(8) Klotz, I. M.; Urquhart, J. M. The binding of organic ions by proteins. Comparison of native and of modified proteins. *J. Am. Chem. Soc.* **1949**, *71*, 1597−1603.

(9) Lund, M. Anisotropic protein−protein interactions due to ion binding. *Colloids Surf., B* **2016**, *137*, 17−21.

(10) Sheinerman, F. B.; Honig, B. On the role of electrostatic interactions in the design of protein−protein interfaces. *J. Mol. Biol.* **2002**, *318*, 161−177.

(11) Berend, K.; van Hulsteijn, L. H.; Gans, R. O. Chloride: the queen of electrolytes? *Eur. J. Intern. Med.* **2012**, *23*, 203−211.

(12) Powers, F. The role of chloride in acid-base balance. *J. Infusion Nurs.* **1999**, *22*, 286.

(13) Yunos, N. M.; Bellomo, R.; Story, D.; Kellum, J. Bench-to-bedside review: chloride in critical illness. *Critical Care* **2010**, *14*, 226.

(14) Koch, S. M.; Taylor, R. W. Chloride ion in intensive care medicine. *Crit. Care Med.* **1992**, *20*, 227−240.

(15) Mason, B. D.; Zhang-van Enk, J.; Zhang, L.; Remmele, R. L., Jr; Zhang, J. Liquid-liquid phase separation of a monoclonal antibody and nonmonotonic influence of Hofmeister anions. *Biophys. J.* **2010**, *99*, 3792−3800.

(16) Ward, R. L.; Cull, M. D. Active site chloride binding in liver alcohol dehydrogenase. *Biochim. Biophys. Acta, Protein Struct.* **1974**, *365*, 281−284.

(17) Winkler, R. Iodine—a potential antioxidant and the role of Iodine/Iodide in health and disease. *Nat. Sci.* **2015**, *7*, 548.

(18) De la Vieja, A.; Santisteban, P. Role of iodide metabolism in physiology and cancer. *Endocr.-Relat. Cancer* **2018**, *25*, R225−R245.

(19) Ahad, F.; Ganie, S. A. Iodine, iodine metabolism and iodine deficiency disorders revisited. *Indian J. Endocrinol. Metab.* **2010**, *14*, 13.

(20) Thomas, E. L.; Aune, T. M. Cofactor role of iodide in peroxidase antimicrobial action against Escherichia coli. *Antimicrob. Agents Chemother.* **1978**, *13*, 1000−1005.

(21) Iwata, A.; Morrison, M. L.; Roth, M. B. Iodide protects heart tissue from reperfusion injury. *PLoS One* **2014**, *9*, e112458.

(22) Fischer, A. J.; Lennemann, N. J.; Krishnamurthy, S.; Pócza, P.; Durairaj, L.; Launspach, J. L.; Rhein, B. A.; Wohlford-Lenane, C.; Lorentzen, D.; Bánfi, B.; McCray, P. B. J. Enhancement of respiratory mucosal antiviral defenses by the oxidation of iodide. *Am. J. Respir. Cell Mol. Biol.* **2011**, *45*, 874−881.

(23) Moreira, L.; Boström, M.; Ninham, B.; Biscaia, E. C.; Tavares, F. W. Hofmeister effects: Why protein charge, pH titration and protein precipitation depend on the choice of background salt solution. *Colloids Surf., A* **2006**, *282*, 457−463.

(24) Hofmeister, F. Zur Lehre von der Wirkung der Salze. *Naunyn-Schmiedeberg's Arch. Pharmacol.* **1888**, *24*, 247−260.

(25) Lo Nostro, P.; Ninham, B. W. Hofmeister phenomena: an update on ion specificity in biology. *Chem. Rev.* **2012**, *112*, 2286−2322.

(26) Williams, R. J. P. Tilden Lecture. The biochemistry of sodium, potassium, magnesium, and calcium. *Q. Rev., Chem. Soc.* **1970**, *24*, 331−365.

(27) Triggle, C. R.; Triggle, D. J. An analysis of the action of cations of the lanthanide series on the mechanical responses of guinea-pig ileal longitudinal muscle. *J. Physiol.* **1976**, *254*, 39−54.

(28) Heffeter, P.; Jakupec, M. A.; Körner, W.; Wild, S.; von Keyserlingk, N. G.; Elbling, L.; Zorbas, H.; Korynevska, A.; Knasmüller, S.; Sutterlüty, H.; Micksche, M.; Keppler, B. K.; Berger, W. Anticancer activity of the lanthanum compound (tris (1, 10-phenanthroline) lanthanum (III)) trithiocyanate (KP772; FFC24). *Biochem. Pharmacol.* **2006**, *71*, 426−440.

(29) Dai, Y.; Li, J.; Li, J.; Yu, L.; Dai, G.; Hu, A.; Yuan, L.; Wen, Z. Effects of rare earth compounds on growth and apoptosis of leukemic cell lines. *In Vitro Cellular & Developmental Biology-Animal* **2002**, *38*, 373−375.

(30) Sato, T.; Hashizume, M.; Hotta, Y.; Okahata, Y. Morphology and proliferation of B16 melanoma cells in the presence of lanthanoid and Al 3+ ions. *BioMetals* **1998**, *11*, 107−112.

(31) Basu, A.; Chakrabarty, K.; Chatterjee, G. C. Neurotoxicity of lanthanum chloride in newborn chicks. *Toxicol. Lett.* **1982**, *14*, 21−25.

(32) Vaccari, A.; Saba, P.; Mocci, I.; Ruiu, S. Lanthanides stimulate (3H) tyramine binding in the rat striatum. *Neurosci. Lett.* **1999**, *261*, 49−52.

(33) Pałasz, A.; Czekaj, P. Toxicological and cytophysiological aspects of lanthanides action. *Acta Biochim. Pol.* **2000**, *47*, 1107−14.

(34) Xu, C.-M.; Zhao, B.; Wang, X.-D.; Wang, Y.-C. Lanthanum relieves salinity-induced oxidative stress in Saussurea involucrata. *Biol. Plant.* **2007**, *51*, 567−570.

(35) Matsarskaia, O.; Roosen-Runge, F.; Lotze, G.; Möller, J.; Mariani, A.; Zhang, F.; Schreiber, F. Tuning phase transitions of aqueous protein solutions by multivalent cations. *Phys. Chem. Chem. Phys.* **2018**, *20*, 27214−27225.

(36) Stubbs, R. S.; Cannan, R. J.; Mitchell, A. W. Selective internal radiation therapy (SIRT) with 90Yttrium microspheres for extensive colorectal liver metastases. *Hepatogastroenterology* **2001**, *48*, 333−337.

(37) Vaughan, A. T.; Keeling, A.; Yankuba, S. The production and biological distribution of yttrium-90 labelled antibodies. *Int. J. Appl. Radiat. Isot.* **1985**, *36*, 803−806.

(38) Webster, T. J.; Ergun, C.; Doremus, R. H.; Bizios, R. Hydroxylapatite with substituted magnesium, zinc, cadmium, and yttrium. II. Mechanisms of osteoblast adhesion. *J. Biomed. Mater. Res.* **2002**, *59*, 312−317.

(39) Fujihara, S.; Akiyama, R. Attractive interaction between macroanions mediated by multivalent cations in biological fluids. *J. Mol. Liq.* **2014**, *200*, 89−94.

(40) Yu, J.; Jackson, N. E.; Xu, X.; Morgenstern, Y.; Kaufman, Y.; Ruths, M.; De Pablo, J. J.; Tirrell, M. Multivalent counterions diminish the lubricity of polyelectrolyte brushes. *Science* **2018**, *360*, 1434−1438.

(41) Wang, X.; Lee, S. Y.; Miller, K.; Welbourn, R.; Stocker, I.; Clarke, S.; Casford, M.; Gutfreund, P.; Skoda, M. W. A. Cation bridging studied by specular neutron reflection. *Langmuir* **2013**, *29*, 5520−5527.

(42) Korkmaz Zirpel, N.; Park, E. J. Trivalent Cation Induced Bundle Formation of Filamentous fd Phages. *Macromol. Biosci.* **2015**, *15*, 1262−1273.

(43) Gurnev, P. A.; Bezrukov, S. M. Inversion of membrane surface charge by trivalent cations probed with a cation-selective channel. *Langmuir* **2012**, *28*, 15824−15830.

(44) Martín-Molina, A.; Rodríguez-Beas, C.; Faraudo, J. Charge reversal in anionic liposomes: experimental demonstration and molecular origin. *Phys. Rev. Lett.* **2010**, *104*, 168103.

(45) Zhang, F.; Skoda, M. W. A.; Jacobs, R. M. J.; Zorn, S.; Martin, R. A.; Martin, C. M.; Clark, G. F.; Weggler, S.; Hildebrandt, A.; Kohlbacher, O.; Schreiber, F. Reentrant condensation of proteins in solution induced by multivalent counterions. *Phys. Rev. Lett.* **2008**, *101*, 148101.

(46) Zhang, F.; Skoda, M. W. A.; Jacobs, R. M. J.; Martin, R. A.; Martin, C. M.; Schreiber, F. Protein interactions studied by SAXS: effect of ionic strength and protein concentration for BSA in aqueous solutions. *J. Phys. Chem. B* **2007**, *111*, 251−259.

(47) Zhang, F.; Roosen-Runge, F.; Sauter, A.; Wolf, M.; Jacobs, R. M.; Schreiber, F. Reentrant condensation, liquid−liquid phase separation and crystallization in protein solutions induced by multivalent metal ions. *Pure Appl. Chem.* **2014**, *86*, 191−202.

(48) Zhang, F.; Weggler, S.; Ziller, M. J.; Ianeselli, L.; Heck, B. S.; Hildebrandt, A.; Kohlbacher, O.; Skoda, M. W. A.; Jacobs, R. M. J.; Schreiber, F. Universality of protein reentrant condensation in solution induced by multivalent metal ions. *Proteins: Struct., Funct., Genet.* **2010**, *78*, 3450−3457.

(49) Ianeselli, L.; Zhang, F.; Skoda, M. W. A.; Jacobs, R. M. J.; Martin, R. A.; Callow, S.; Prévost, S.; Schreiber, F. Protein- protein interactions in ovalbumin solutions studied by small-angle scattering: effect of ionic strength and the chemical nature of cations. *J. Phys. Chem. B* **2010**, *114*, 3776−3783.

(50) Sauter, A.; Roosen-Runge, F.; Zhang, F.; Lotze, G.; Jacobs, R. M. J.; Schreiber, F. Real-time observation of nonclassical protein crystallization kinetics. *J. Am. Chem. Soc.* **2015**, *137*, 1485−1491.

(51) Andrade, J. D.; Hlady, V. *Biopolymers/Non-Exclusion HPLC*; Springer, 1986; pp 1−63.

(52) Majorek, K. A.; Porebski, P. J.; Dayal, A.; Zimmerman, M. D.; Jablonska, K.; Stewart, A. J.; Chruszcz, M.; Minor, W. Structural and immunologic characterization of bovine, horse, and rabbit serum albumins. *Mol. Immunol.* **2012**, *52*, 174−182.

(53) Sperling, C.; Schweiss, R. B.; Streller, U.; Werner, C. In vitro hemocompatibility of self-assembled monolayers displaying various functional groups. *Biomaterials* **2005**, *26*, 6547−6557.

(54) Jin, J.; Zhang, C.; Jiang, W.; Luan, S.; Yang, H.; Yin, J.; Stagnaro, P. Melting grafting polypropylene with hydrophilic monomers for improving hemocompatibility. *Colloids Surf., A* **2012**, *407*, 141−149.

(55) Werner, C.; Maitz, M. F.; Sperling, C. Current strategies towards hemocompatible coatings. *J. Mater. Chem.* **2007**, *17*, 3376−3384.

(56) Colman, R. W.; Schmaier, A. H. Contact system: a vascular biology modulator with anticoagulant, profibrinolytic, antiadhesive, and proinflammatory attributes. *Blood. Blood* **1997**, *90*, 3819−3843.

(57) Colman, R. W. Surface-mediated defense reactions. The plasma contact activation system. *J. Clin. Invest.* **1984**, *73*, 1249−1253.

(58) Braun, M. K.; Wolf, M.; Matsarskaia, O.; Da Vela, S.; Roosen-Runge, F.; Sztucki, M.; Roth, R.; Zhang, F.; Schreiber, F. Strong isotope effects on effective interactions and phase behavior in protein solutions in the presence of multivalent ions. *J. Phys. Chem. B* **2017**, *121*, 1731−1739.

(59) Covington, A. K.; Paabo, M.; Robinson, R. A.; Bates, R. G. Use of the glass electrode in deuterium oxide and the relation between the standardized pD (paD) scale and the operational pH in heavy water. *Anal. Chem.* **1968**, *40*, 700−706.

(60) Mora, M. F.; Wehmeyer, J. L.; Synowicki, R.; Garcia, C. D. *Biological Interactions on Materials Surfaces*; Springer, 2009; pp 19−41.

(61) Den Boer, J. H. W. G. *Spectroscopic infrared ellipsometry: components, calibration and application*; Technische Universiteit Eindhoven, 1992.

(62) Cuypers, P. A.; Hermens, W. T.; Hemker, H. C. Ellipsometry as a tool to study protein films at liquid-solid interfaces. *Anal. Biochem.* **1978**, *84*, 56−67.

(63) Scarangella, A.; Soumbo, M.; Villeneuve-Faure, C.; Mlayah, A.; Bonafos, C.; Monje, M.-C.; Roques, C.; Makasheva, K. Adsorption properties of BSA and DsRed proteins deposited on thin SiO2 layers: optically non-absorbing versus absorbing proteins. *Nanotechnology* **2018**, *29*, 115101.

(64) Balevicius, Z.; Paulauskas, A.; Plikusiene, I.; Mikoliunaite, L.; Bechelany, M.; Popov, A.; Ramanavicius, A.; Ramanaviciene, A. Towards the application of Al 2 O 3/ZnO nanolaminates in immunosensors: total internal reflection spectroscopic ellipsometry based evaluation of BSA immobilization. *J. Mater. Chem. C* **2018**, *6*, 8778−8783.

(65) Nejadnik, M. R.; Garcia, C. D. Staining proteins: A simple method to increase the sensitivity of ellipsometric measurements in adsorption studies. *Colloids Surf, B* **2011**, *82*, 253−257.

(66) Tsargorodskaya, A.; Nabok, A. V.; Ray, A. K. Ellipsometric study of the adsorption of bovine serum albumin into porous silicon. *Nanotechnology* **2004**, *15*, 703.

(67) Reviakine, I.; Johannsmann, D.; Richter, R. P. Hearing what you cannot see and visualizing what you hear: interpreting quartz crystal microbalance data from solvated interfaces. *Anal. Chem.* **2011**, *83*, 8838−8848.

(68) Voinova, M. V.; Rodahl, M.; Jonson, M.; Kasemo, B. Viscoelastic acoustic response of layered polymer films at fluid-solid interfaces: continuum mechanics approach. *Phys. Scr.* **1999**, *59*, 391.

(69) Zhang, B.; Wang, Q. Quartz crystal microbalance with dissipation. *Nanotechnology Research Methods for Food and Bioproducts* **2012**, 181.

(70) Vogt, B. D.; Lin, E. K.; Wu, W.-l.; White, C. C. Effect of film thickness on the validity of the Sauerbrey equation for hydrated polyelectrolyte films. *J. Phys. Chem. B* **2004**, *108*, 12685−12690.

(71) Feiler, A. A.; Sahlholm, A.; Sandberg, T.; Caldwell, K. D. Adsorption and viscoelastic properties of fractionated mucin (BSM) and bovine serum albumin (BSA) studied with quartz crystal microbalance (QCM-D). *J. Colloid Interface Sci.* **2007**, *315*, 475−481.

(72) Rojas, E.; Gallego, M.; Reviakine, I. Effect of sample heterogeneity on the interpretation of quartz crystal microbalance data: impurity effects. *Anal. Chem.* **2008**, *80*, 8982−8990.

(73) Macakova, L.; Blomberg, E.; Claesson, P. M. Effect of adsorbed layer surface roughness on the QCM-D response: focus on trapped water. *Langmuir* **2007**, *23*, 12436−12444.

(74) Rodenhausen, K. B.; Schubert, M. Virtual separation approach to study porous ultra-thin films by combined spectroscopic ellipsometry and quartz crystal microbalance methods. *Thin Solid Films* **2011**, *519*, 2772−2776.

(75) Fries, M. R.; Stopper, D.; Skoda, M. W. A.; Blum, M.; Kertzscher, C.; Hinderhofer, A.; Zhang, F.; Jacobs, R. M. J.; Roth, R.; Schreiber, F. Enhanced protein adsorption upon bulk phase separation. *Sci. Rep.* **2020**, *10*, 10349.

(76) Tantipolphan, R.; Rades, T.; McQuillan, A. J.; Medlicott, N. J. Adsorption of bovine serum albumin (BSA) onto lecithin studied by attenuated total reflectance Fourier transform infrared (ATR-FTIR) spectroscopy. *Int. J. Pharm.* **2007**, *337*, 40−47.

(77) Chittur, K. K. FTIR/ATR for protein adsorption to biomaterial surfaces. *Biomaterials* **1998**, *19*, 357−369.

(78) Braun, M. K.; Sauter, A.; Matsarskaia, O.; Wolf, M.; Roosen-Runge, F.; Sztucki, M.; Roth, R.; Zhang, F.; Schreiber, F. Reentrant phase behavior in protein solutions induced by multivalent salts: strong effect of anions Cl⁻ versus NO₃⁻. *J. Phys. Chem. B* **2018**, *122*, 11978−11985.

(79) Roosen-Runge, F.; Zhang, F.; Schreiber, F.; Roth, R. Ion-activated attractive patches as a mechanism for controlled protein interactions. *Sci. Rep.* **2015**, *4*, 7016.

(80) Vliegenthart, G. A.; Lekkerkerker, H. N. W. Predicting the gas−liquid critical point from the second virial coefficient. *J. Chem. Phys.* **2000**, *112*, 5364−5369.

(81) Schomäcker, K.; Mocker, D.; Münze, R.; Beyer, G.-J. Stabilities of lanthanide-protein complexes. *International Journal of Radiation Applications and Instrumentation. Part A. Applied Radiation and Isotopes* **1988**, *39*, 261−264.

(82) Smolka, G. E.; Birnbaum, E. R.; Darnall, D. W. Rare earth metal ions as substitutes for the calcium ion in Bacillus subtilis α-Amylase. *Biochemistry* **1971**, *10*, 4556−4561.

(83) Gomez, J. E.; Birnbaum, E. R.; Darnall, D. W. Metal ion acceleration of the conversion of trypsinogen to trypsin. Lanthanide ions as calcium ion substitutes. *Biochemistry* **1974**, *13*, 3745−3750.

(84) Mulqueen, P.; Tingey, J. M.; Horrocks, W. D., Jr Characterization of lanthanide (III) ion binding to calmodulin using luminescence spectroscopy. *Biochemistry* **1985**, *24*, 6639−6645.

(85) Marcus, Y. Individual ionic surface tension increments in aqueous solutions. *Langmuir* **2013**, *29*, 2881−2888.

(86) Marcus, Y. Viscosity B-coefficients, structural entropies and heat capacities, and the effects of ions on the structure of water. *J. Solution Chem.* **1994**, *23*, 831−848.

(87) Jenkins, H. D. B.; Marcus, Y. Viscosity B-coefficients of ions in solution. *Chem. Rev.* **1995**, *95*, 2695−2724.

(88) Marcus, Y. Effect of ions on the structure of water: structure making and breaking. *Chem. Rev.* **2009**, *109*, 1346−1370.

(89) Collins, K. D. Charge density-dependent strength of hydration and biological structure. *Biophys. J.* **1997**, *72*, 65−76.

(90) Carr, C. W. Studies on the binding of small ions in protein solutions with the use of membrane electrodes. I. The binding of the chloride ion and other inorganic anions in solutions of serum albumin. *Arch. Biochem. Biophys.* **1952**, *40*, 286−294.

(91) Marcus, Y. *Ion properties*; CRC Press, 1997.

(92) Zhang, Y.; Cremer, P. S. Interactions between macromolecules and ions: the Hofmeister series. *Curr. Opin. Chem. Biol.* **2006**, *10*, 658−663.

(93) Yamasaki, M.; Yano, H.; Aoki, K. Differential scanning calorimetric studies on bovine serum albumin: II. Effects of neutral salts and urea. *Int. J. Biol. Macromol.* **1991**, *13*, 322−328.

(94) Cacace, M. G.; Landau, E. M.; Ramsden, J. J. The Hofmeister series: salt and solvent effects on interfacial phenomena. *Q. Rev. Biophys.* **1997**, *30*, 241−277.

(95) Okur, H. I.; Hladilkova, J.; Rembert, K. B.; Cho, Y.; Heyda, J.; Dzubiella, J.; Cremer, P. S.; Jungwirth, P. Beyond the Hofmeister series: Ion-specific effects on proteins and their biological functions. *J. Phys. Chem. B* **2017**, *121*, 1997.

(96) Washabaugh, M. W.; Collins, K. D. The systematic characterization by aqueous column chromatography of solutes which affect protein stability. *J. Biol. Chem.* **1986**, *261*, 12477−12485.

(97) Collins, K. D.; Washabaugh, M. W. The Hofmeister effect and the behaviour of water at interfaces. *Q. Rev. Biophys.* **1985**, *18*, 323−422.

(98) Maruyama, T.; Katoh, S.; Nakajima, M.; Nabetani, H.; Abbott, T. P.; Shono, A.; Satoh, K. FT-IR analysis of BSA fouled on ultrafiltration and microfiltration membranes. *J. Membr. Sci.* **2001**, *192*, 201−207.

(99) Roosen-Runge, F.; Heck, B. S.; Zhang, F.; Kohlbacher, O.; Schreiber, F. Interplay of pH and binding of multivalent metal ions: charge inversion and reentrant condensation in protein solutions. *J. Phys. Chem. B* **2013**, *117*, 5777−5787.

(100) Longsworth, L. G.; Jacobsen, C. F. An Electrophoretic Study of the Binding of Salt Ions by β-Lactoglobulin and Bovine Serum Albumin. *J. Phys. Chem.* **1949**, *53*, 126−134.

(101) Collins, K. D. Ions from the Hofmeister series and osmolytes: effects on proteins in solution and in the crystallization process. *Methods* **2004**, *34*, 300−311.

(102) Vaney, M.; Broutin, I.; Retailleau, P.; Douangamath, A.; Lafont, S.; Hamiaux, C.; Prangé, T.; Ducruix, A.; Riès-Kautt, M. Structural effects of monovalent anions on polymorphic lysozyme crystals. *Acta Crystallogr., Sect. D: Biol. Crystallogr.* **2001**, *57*, 929−940.

(103) Lund, M.; Jungwirth, P.; Woodward, C. E. Ion specific protein assembly and hydrophobic surface forces. *Phys. Rev. Lett.* **2008**, *100*, 258105.

(104) Scatchard, G.; Coleman, J. S.; Shen, A. L. Physical Chemistry of Protein Solutions. VII. The Binding of Some Small Anions to Serum Albumin. *J. Am. Chem. Soc.* **1957**, *79*, 12−20.

(105) Scatchard, G.; Scheinberg, I. H.; Armstrong, S. H., Jr Physical Chemistry of Protein Solutions. IV. The Combination of Human Serum Albumin with Chloride Ion. *J. Am. Chem. Soc.* **1950**, *72*, 535−540.

(106) Scatchard, G.; Scheinberg, I. H.; Armstrong, S. H., Jr Physical chemistry of protein solutions. v. the combination of human serum albumin with thiocyanate ion. *J. Am. Chem. Soc.* **1950**, *72*, 540−546.

(107) Norne, J. E.; Hjalmarsson, S. G.; Lindman, B.; Zeppezauer, M. Anion binding properties of human serum albumin from halide ion quadrupole relaxation. *Biochemistry* **1975**, *14*, 3401−3408.

(108) Lund, M.; Vácha, R.; Jungwirth, P. Specific ion binding to macromolecules: effects of hydrophobicity and ion pairing. *Langmuir* **2008**, *24*, 3387−3391.

(109) Lund, M.; Vrbka, L.; Jungwirth, P. Specific ion binding to nonpolar surface patches of proteins. *J. Am. Chem. Soc.* **2008**, *130*, 11582−11583.

(110) Fox, J. M.; Kang, K.; Sherman, W.; Héroux, A.; Sastry, G. M.; Baghbanzadeh, M.; Lockett, M. R.; Whitesides, G. M. Interactions between Hofmeister anions and the binding pocket of a protein. *J. Am. Chem. Soc.* **2015**, *137*, 3859−3866.

(111) Dzubiella, J. Salt-specific stability and denaturation of a short salt-bridge-forming α-helix. *J. Am. Chem. Soc.* **2008**, *130*, 14000−14007.

(112) Karush, F. Heterogeneity of the binding sites of bovine serum albumin. *J. Am. Chem. Soc.* **1950**, *72*, 2705−2713.

(113) Nozaki, Y.; Reynolds, J. A.; Tanford, C. The interaction of a cationic detergent with bovine serum albumin and other proteins. *J. Biol. Chem.* **1974**, *249*, 4452−4459.

(114) Peters, T., Jr. *Advances in Protein Chemistry*; Elsevier, 1985; Vol. 37; pp 161−245.

(115) Rembert, K. B.; Paterova, J.; Heyda, J.; Hilty, C.; Jungwirth, P.; Cremer, P. S. Molecular mechanisms of ion-specific effects on proteins. *J. Am. Chem. Soc.* **2012**, *134*, 10039−10046.

(116) Ayranci, E.; Duman, O. Binding of fluoride, bromide and iodide to bovine serum albumin, studied with ion-selective electrodes. *Food Chem.* **2004**, *84*, 539−543.

(117) Zhang, F.; Zocher, G.; Sauter, A.; Stehle, T.; Schreiber, F. Novel approach to controlled protein crystallization through ligandation of yttrium cations. *J. Appl. Crystallogr.* **2011**, *44*, 755−762.

(118) Richert, M. E.; Gochev, G. G.; Braunschweig, B. Specific ion effects of trivalent cations on the structure and charging state of β-lactoglobulin adsorption layers. *Langmuir* **2019**, *35*, 11299−11307.

(119) Matsarskaia, O.; Braun, M. K.; Roosen-Runge, F.; Wolf, M.; Zhang, F.; Roth, R.; Schreiber, F. Cation-induced hydration effects cause lower critical solution temperature behavior in protein solutions. *J. Phys. Chem. B* **2016**, *120*, 7731−7736.

(120) Wood, S. A. The aqueous geochemistry of the rare-earth elements and yttrium: 1. Review of available low-temperature data for inorganic complexes and the inorganic REE speciation of natural waters. *Chem. Geol.* **1990**, *82*, 159−186.

(121) Wood, S. A. The aqueous geochemistry of the rare-earth elements and yttrium: 2. Theoretical predictions of speciation in hydrothermal solutions to 350 C at saturation water vapor pressure. *Chem. Geol.* **1990**, *88*, 99−125.

(122) Rudolph, W. W.; Irmer, G. Hydration and ion pair formation in aqueous Y^{3+}−salt solutions. *Dalton Transactions* **2015**, *44*, 18492−18505.

(123) Rudolph, W. W.; Irmer, G. Hydration and ion pair formation in common aqueous La (III) salt solutions−a Raman scattering and DFT study. *Dalton Transactions* **2015**, *44*, 295−305.

(124) Takahashi, R.; Ishiguro, S.-I. Inner-sphere and outer-sphere complexes of yttrium (III), lanthanum (III), neodymium (III), terbium (III) and thulium (III) with halide ions in N, N-dimethylformamide. *J. Chem. Soc., Faraday Trans.* **1991**, *87*, 3379−3383.

(125) Dzubiella, J. Salt-specific stability of short and charged alanine-based α-helices. *J. Phys. Chem. B* **2009**, *113*, 16689−16694.

(126) Fries, M. R.; Stopper, D.; Braun, M. K.; Hinderhofer, A.; Zhang, F.; Jacobs, R. M. J.; Skoda, M. W. A.; Hansen-Goos, H.; Roth, R.; Schreiber, F. Multivalent-ion-activated protein adsorption reflecting bulk reentrant behavior. *Phys. Rev. Lett.* **2017**, *119*, 228001.

(127) Kubiak-Ossowska, K.; Tokarczyk, K.; Jachimska, B.; Mulheran, P. A. Bovine serum albumin adsorption at a silica surface explored by simulation and experiment. *J. Phys. Chem. B* **2017**, *121*, 3975−3986.

(128) Tiraferri, A.; Maroni, P.; Borkovec, M. Adsorption of polyelectrolytes to like-charged substrates induced by multivalent counterions as exemplified by poly (styrene sulfonate) and silica. *Phys. Chem. Chem. Phys.* **2015**, *17*, 10348−10352.

(129) Susi, H.; Byler, D. M. Fourier deconvolution of the amide I Raman band of proteins as related to conformation. *Appl. Spectrosc.* **1988**, *42*, 819−826.

(130) Jordan, J. L.; Fernandez, E. J. QCM-D sensitivity to protein adsorption reversibility. *Biotechnol. Bioeng.* **2008**, *101*, 837−842.

(131) Rodahl, M.; Höök, F.; Fredriksson, C.; Keller, C. A.; Krozer, A.; Brzezinski, P.; Voinova, M.; Kasemo, B. Simultaneous frequency and dissipation factor QCM measurements of biomolecular adsorption and cell adhesion. *Faraday Discuss.* **1997**, *107*, 229−246.

(132) Voinova, M. V.; Jonson, M.; Kasemo, B. 'Missing mass' effect in biosensor's QCM applications. *Biosens. Bioelectron.* **2002**, *17*, 835−841.

(133) Liu, S. X.; Kim, J.-T. Application of Kevin—Voigt model in quantifying whey protein adsorption on polyethersulfone using QCM-D. *JALA* **2009**, *14*, 213−220.

(134) Steinem, C.; Janshoff, A. *Piezoelectric sensors*; Springer Science & Business Media, 2007; Vol. 5.

(135) Bingen, P.; Wang, G.; Steinmetz, N. F.; Rodahl, M.; Richter, R. P. Solvation effects in the QCM-D response to biomolecular adsorption—a phenomenological approach. *Anal. Chem.* **2008**, *80*, 8880−8890.